

Energy shift of magnons in a ferromagnetic spinor-dipolar Bose-Einstein condensate

Hiroki Saito¹ and Masaya Kunimi¹

¹*Department of Engineering Science, University of Electro-Communications, Tokyo 182-8585, Japan*
(Dated: June 25, 2018)

Motivated by the recent experiment performed by the Berkeley group [G. E. Marti *et al.*, Phys. Rev. Lett. **113**, 155302 (2014)], we consider the dynamics of magnons in a spin-1 spinor-dipolar Bose-Einstein condensate, using mean-field theory. We show that the effective mass of a magnon is increased by the magnetic dipole-dipole interaction, as observed in the experiment. The magnon mass is also decreased by changing the direction of the magnetic field. The increase and decrease in the magnon mass manifest themselves in the acceleration of the magnons.

PACS numbers: 67.85.Fg, 03.75.Mn, 03.75.Kk, 75.30.Ds

Due to the long-range and anisotropic properties of the magnetic dipole-dipole interaction (MDDI), Bose-Einstein condensates (BECs) of ultracold atoms with a magnetic dipole moment exhibit a variety of intriguing phenomena in experiments, including anisotropic deformation and excitation of the condensate [1–4], instability in a prolate system [5, 6], *d*-wave collapse and expansion [7–9], and spinor-dipolar dynamics [10, 11]. Many theoretical investigations have also been made of supersolidity [12], the roton spectrum [13–16], rotating properties [17–21], soliton stability [22–24], the Einstein-de Haas effect [25–27], spin-texture formation [28–32], Rosensweig instability [33], and various spin dynamics [34, 35].

Observation and identification of dipolar effects in a spin-1 ⁸⁷Rb BEC are difficult [36, 37] compared with the cases of ⁵²Cr, ¹⁶⁴Dy, and ¹⁶⁸Er BECs, since the MDDI of spin-1 ⁸⁷Rb atoms is much smaller than the characteristic energies in the system. Recently, using the technique of precise *in situ* measurement of spin states, the Berkeley group observed magnon dynamics in a spin-1 ⁸⁷Rb BEC [38]. Although the mean-field theory without MDDI predicts that the dispersion relation of a magnon is the same as that of a free atom [39, 40], the experimental result significantly deviates from the prediction and the effective mass of a magnon is measured to be $\simeq 3\%$ larger than that of a free atom. This deviation is much larger than the quantum many-body correction [41]. The authors of Ref. [38] attribute the deviation to the MDDI, which has yet to be evaluated by quantitative theoretical analysis.

In this Rapid Communication, we investigate the effect of the MDDI on the dynamics of a magnon in the same setup as was used by the Berkeley experiment [38]. Using the mean-field theory with the MDDI, we confirm that the dispersion relation and the effective mass of a magnon deviate from those of a free atom, as observed in the experiment. We also propose a simple modification to the experiment: when the direction of the magnetic field is changed from the long axis to the tight axis of the oblate condensate, the magnon mass is found to be decreased. We show that the increase and decrease in the magnon mass affect the acceleration of magnons in the magnetic

field gradient.

We employ the mean-field approximation to study the dynamics of a spin-1 BEC with MDDI. In the experiment [38], a magnetic field of 115 mG is applied (we take its direction as the *z* axis), which induces the Larmor precession at a frequency of $\simeq 80$ kHz. This time scale is much faster than that of the condensate dynamics, and therefore the MDDI can be time-averaged with respect to the Larmor precession [42, 43]. The macroscopic wave functions $\psi_m(\mathbf{r}, t)$ for the magnetic sublevels $m = \pm 1$ and 0 thus obey the nonlocal Gross-Pitaevskii (GP) equation given by

$$\begin{aligned} i\hbar \frac{\partial \psi_m}{\partial t} = & \left(-\frac{\hbar^2}{2M} \nabla^2 + V + g_0 \rho + m^2 q \right) \psi_m \\ & + g_1 \mathbf{F} \cdot \sum_{m'} \mathbf{f}_{mm'} \psi_{m'} \\ & + g_d \int d\mathbf{r}' \frac{1 - 3 \cos^2 \theta}{|\mathbf{r} - \mathbf{r}'|^3} \\ & \times \sum_{m'} [3F_z(\mathbf{r}') f_{mm'}^z - \mathbf{F}(\mathbf{r}') \cdot \mathbf{f}_{mm'}] \psi_{m'}(\mathbf{r}), \end{aligned} \quad (1)$$

where M is the mass of an ⁸⁷Rb atom, $V = M(\omega_x^2 x^2 + \omega_y^2 y^2 + \omega_z^2 z^2)/2$ is the harmonic trap potential, $\rho = \sum_m |\psi_m|^2$ is the total density, q is the quadratic Zeeman shift, \mathbf{f} is the vector of spin-1 matrices, $\mathbf{F} = \sum_{mm'} \psi_m^* \mathbf{f} \psi_{m'}$ is the spin density, and θ is the angle between $\mathbf{r} - \mathbf{r}'$ and the *z* axis. The interaction coefficients in Eq. (1) are defined as $g_0 = 4\pi\hbar^2(a_0 + 2a_2)/(3M)$, $g_1 = 4\pi\hbar^2(a_2 - a_0)/(3M)$, and $g_d = \mu_0(\mu_B/2)^2/(8\pi)$, where a_S is the *s*-wave scattering length for two colliding atoms with total spin S , μ_0 is the vacuum permeability, and μ_B is the Bohr magneton. The trap frequencies are taken to be $(\omega_x, \omega_y, \omega_z)/2\pi = (9, 300, 4)$ Hz, as in the experiment. The wave function is normalized as $\int \rho d\mathbf{r} = N$, where N is the number of atoms. We take $N = 3.2 \times 10^6$ so that the peak density at the center of the trap becomes the experimental value, 1.5×10^{14} cm⁻³. The quadratic Zeeman shift is $q \simeq \hbar \times 1$ Hz for the magnetic field of 115 mG, which does not affect the following results.

The initial state is the ground state of the $m = -1$

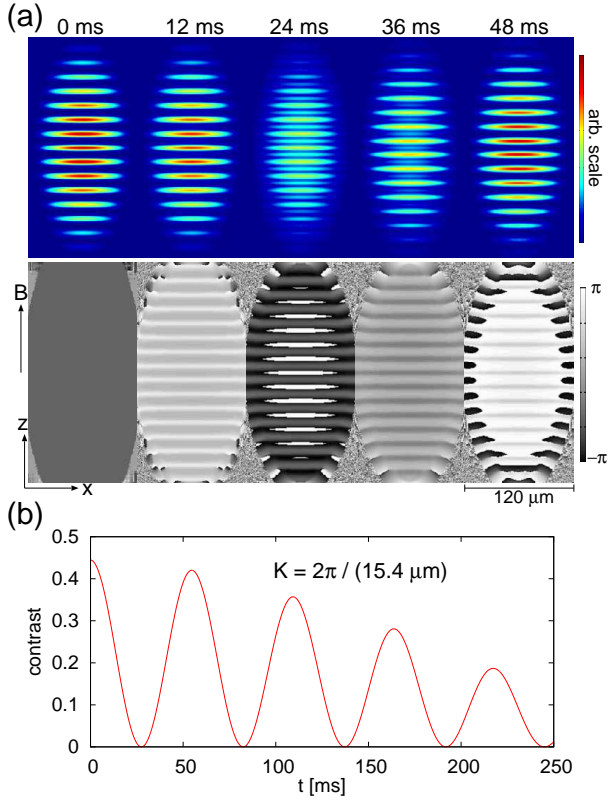


FIG. 1: (color online) (a) Time evolution of the column density profile $\int |\psi_0|^2 dy$ (upper panels) and cross-sectional phase profile $\arg \psi_0(y=0)$ (lower panels). See Supplemental Material for a movie of the dynamics of the column density profile [45]. (b) Time evolution of the fringe contrast. The wave number of the excited magnons in (a) and (b) is $K = 2\pi/(15.4\mu\text{m})$.

component, $\psi_{-1} \equiv \Psi_{-1}$, with $\psi_1 = \psi_0 = 0$. Magnons with wave numbers $\pm K$ are excited as

$$\psi_m(\mathbf{r}) = \{\exp[-i\epsilon(1 + \cos Kz)f^x]\}_{m,-1}\Psi_{-1}(\mathbf{r}), \quad (2)$$

where $\epsilon \ll 1$ is a constant. The operator acting on Ψ_{-1} in Eq. (2) generates magnons propagating in the $\pm z$ directions, which is the long axis of the oblate condensate. Since the experimental results are extrapolated to $\epsilon \rightarrow 0$ [38], we typically take $\epsilon = 0.01$ in the numerical calculations; this is small enough and the numerical results are insensitive to the value of ϵ .

We numerically solve Eq. (1) using the pseudospectral method [44]. The initial ground state Ψ_{-1} is prepared by the imaginary-time propagation method, in which i on the left-hand side of Eq. (1) is replaced by -1 . The convolution integral in the MDDI term is calculated using the fast Fourier transform. The numerical mesh is typically $256 \times 16 \times 512$.

Figure 1(a) shows the time evolution of the density and phase profiles of the $m = 0$ component, which approximately represent the magnon density and the tilting direction of the spin vector, respectively. Assuming a uni-

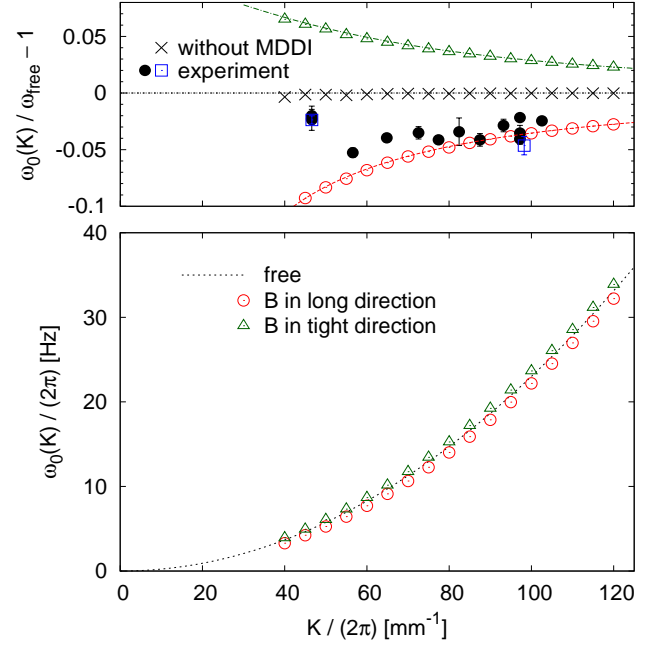


FIG. 2: (color online) Dispersion relation of a magnon, where $\omega_0(K) \equiv \omega(K) - \omega(0)$. The red circles and green triangles are obtained by numerically solving the GP equation, where in the former, the magnetic field is in the direction of the long axis of the oblate condensate, and in the latter, the magnetic field is in the direction of the tight axis. The black crosses are the numerical result without the MDDI. The black dotted curve shows the dispersion relation for a free atom. The black solid circles and the blue squares are the experimental data, where the former was obtained from a single tipping angle of the spin and the latter was obtained from several tipping angles [38]. The red dashed and green dot-dashed curves are obtained from Eq. (6).

form system, the wave function of the $m = 0$ component produced by Eq. (2) is $\psi_0 \propto 1 + \cos Kz$, which evolves as $e^{-i\omega(0)t} + e^{-i\omega(K)t} \cos Kz$, giving the density

$$|\psi_0|^2 \propto 1 + \cos^2 Kz + 2 \cos \omega_0(K)t \cos Kz \quad (3)$$

with $\omega_0(K) \equiv \omega(K) - \omega(0)$. The fringes of $|\psi_0|^2$ in Fig. 1(a) thus has a pitch of $2\pi/K$ for $\cos \omega_0(K)t \simeq \pm 1$ ($t = 0$ and 48 ms) and $2\pi/(2K)$ for $\cos \omega_0(K)t \simeq 0$ ($t = 24$ ms). Figure 1(b) shows the fringe contrast defined by $|\int e^{-iKz} D(z) dz|^2 / |\int D(z) dz|^2$, where $D(z) \equiv \int |\psi_0|^2 dx dy$. From Eq. (3), the fringe contrast becomes $(2/3)^2 \cos^2 \omega_0(K)t$ for a uniform system. The decay in the oscillation amplitude in Fig. 1(b) is mainly due to the inhomogeneity of the system.

Fitting the fringe contrast to a function $[(2/3)^2 - at - bt^2] \cos^2 \omega t$ with fitting parameters a , b , and ω [46], we obtain the red circles in Fig. 2. As observed in the experiment [38], the dispersion curve lies below that of a free atom (black dotted line in Fig. 2). In the upper panel of Fig. 2, we find that the experimental data are in reasonable agreement with our numerical result. The

crosses in Fig. 2 are obtained by solving the GP equation without the MDDI, and these almost coincide with the dispersion relation of a free atom, indicating that there is little change in the dispersion curve due to the finite-size effect of the trapped system.

To understand the frequency shift obtained above, we consider a linear approximation of Eq. (1). Substituting $\psi_{-1} = \Psi_{-1} + \delta\psi_{-1}$, $\psi_0 = \delta\psi_0$, and $\psi_1 = \delta\psi_1$ into Eq. (1), and taking the first order of $\delta\psi_m$, we obtain

$$i\hbar \frac{\partial \delta\psi_0}{\partial t} = \left(-\frac{\hbar^2}{2M} \nabla^2 + V \right) \delta\psi_0 - g_d \int d\mathbf{r}' \frac{1 - 3 \cos^2 \theta}{|\mathbf{r} - \mathbf{r}'|^3} \Psi_{-1}^*(\mathbf{r}') \Psi_{-1}(\mathbf{r}) \delta\psi_0(\mathbf{r}'). \quad (4)$$

For a uniform system without the MDDI, Eq. (4) reduces to $i\hbar \partial \delta\psi_0 / \partial t = -\hbar^2 / (2M) \nabla^2 \delta\psi_0$, which gives the dispersion relation for a free atom, $\omega(K) = \hbar K^2 / (2M)$. To evaluate the frequency shift by the MDDI, we assume that $\delta\psi_0$ has the same profile as that of Ψ_{-1} :

$$\delta\psi_0(\mathbf{r}, t) = e^{i\mathbf{K} \cdot \mathbf{r}} \Psi_{-1}(\mathbf{r}) u_0(t), \quad (5)$$

where \mathbf{K} is the wave vector of magnons. Substituting Eq. (5) into Eq. (4), multiplying by $e^{-i\mathbf{K} \cdot \mathbf{r}} \Psi_{-1}^*$, and integrating with respect to \mathbf{r} , we obtain

$$i\hbar u_0(t) = \left[\frac{1}{N} \int d\mathbf{r} \Psi_{-1} \left(-\frac{\hbar^2}{2M} \nabla^2 + V \right) \Psi_{-1} + \frac{\hbar^2 K^2}{2M} + \frac{4\pi g_d}{3N} \int \frac{d\mathbf{k}}{(2\pi)^3} (1 - 3 \cos^2 \alpha) |\phi(\mathbf{k} - \mathbf{K})|^2 \right] u_0(t), \quad (6)$$

where α is the angle between \mathbf{k} and the direction of the magnetic field, and $\phi(\mathbf{k}) \equiv \int d\mathbf{r} \exp(-i\mathbf{k} \cdot \mathbf{r}) |\Psi_{-1}|^2$. The first term in the square bracket in Eq. (6) is a constant that does not contribute to $\omega_0(K)$. The second term gives the dispersion relation of a free atom. The K dependence of the third term determines the MDDI effect on $\omega_0(K)$. The red dashed curve in Fig. 2 shows the frequency shift obtained from Eq. (6), where we used the numerically obtained Ψ_{-1} to calculate the MDDI term in Eq. (6). The frequency shift obtained from Eq. (6) is in good agreement with that obtained from the full GP equation.

If we take a Gaussian wave function as Ψ_{-1} , we have

$$|\phi(\mathbf{k} - K\hat{z})|^2 = N e^{-[d_x^2 k_x^2 + d_y^2 k_y^2 + d_z^2 (k_z - K)^2] / 2}, \quad (7)$$

where \hat{z} is the unit vector in the z direction, and d_x , d_y , and d_z are Gaussian widths. Suppose that $d_z \gg K^{-1}$, Eq. (7) is approximated by $|\phi(\mathbf{k} - K\hat{z})|^2 \propto \delta(k_z - K)$, and therefore, $1 - 3 \cos^2 \alpha \sim 1 - 3K^2 / (K^2 + k_x^2 + k_y^2)$. The MDDI integral in Eq. (6) is thus a decreasing function of K and hence the frequency shift is negative [47].

We propose to change the direction of the magnetic field from the long axis to the tight axis of the oblate

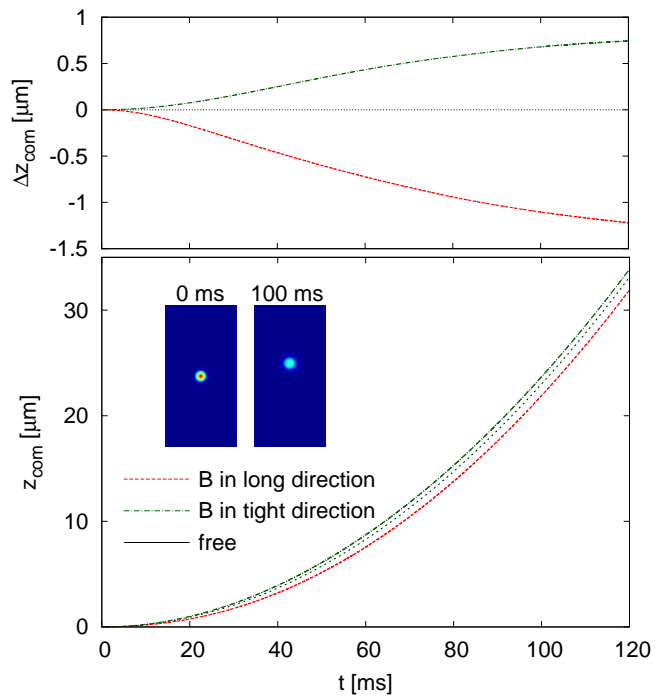


FIG. 3: (color online) Time evolution of the position z_{com} of the center of mass of locally excited magnons, where the Larmor frequency has a gradient of 1 kHz/mm in the z direction. The magnetic field is in the direction of the long axis (red dashed curve) or in the direction of the tight axis (green dot-dashed curve). The black dotted curve shows the motion of a free atom z_{free} . The upper panel shows $\Delta z_{\text{com}} = z_{\text{com}} - z_{\text{free}}$. The insets are snapshots of the column density profile of the $m = 0$ component at $t = 0$ and 100 ms, where the window is the same as in Fig. 1(a). The dynamics of the column density profile is provided as Supplemental Material [45].

BEC (i.e., from the z direction to the y direction). The quantization axis of the spin is always taken to be in the direction of the magnetic field; the spin is initially in the $-y$ direction. The green triangles in Fig. 2 are obtained by numerically solving the GP equation with fitting of the fringe contrast, and the green dot-dashed curve in Fig. 2 is obtained from Eq. (6). The dispersion relation deviates to the upper side of that of a free atom, which indicates that the effective mass of a magnon decreases, contrary to the case in which the magnetic field is in the direction of the long axis. From the upper panel of Fig. 2, we see that the effective mass of a magnon is a few percent smaller than the mass of a free atom. In a similar manner as the above Gaussian approximation, we have $1 - 3 \cos^2 \alpha \sim 1 - 3k_y^2 / (K^2 + k_x^2 + k_y^2)$, and therefore the MDDI integral in Eq. (6) is an increasing function of K , giving the positive frequency shift.

In the experiment [38], the effect of the heavy magnon mass on the acceleration dynamics was not observed due to a systematic error. To clarify the effect of the MDDI on the acceleration dynamics of magnons, we investigate the same situation numerically. The magnetic field

gradient is applied along the long axis of the condensate; this produces the gradient of the Larmor frequency, $\partial_z f_{\text{Larmor}}$. In the initial state, localized magnons are excited as

$$\psi_m(\mathbf{r}) = \{\exp[-i\epsilon\epsilon^{-(x^2+z^2)/\sigma^2}]f^x\}_{m,-1}\Psi_{-1}(\mathbf{r}), \quad (8)$$

where $\epsilon = 0.01$ and $\sigma = 12 \mu\text{m}$. Figure 3 shows the time evolution of the position of the center of mass, $\mathbf{r}_{\text{com}} = \int \mathbf{r}|\psi_0|^2 d\mathbf{r} / \int |\psi_0|^2 d\mathbf{r}$; this exhibits the parabolic acceleration of magnons in the direction of the field gradient, as observed in the experiment. The deviations from the motion of a free atom are shown in the upper panel of Fig. 3. As expected, the acceleration is suppressed when the magnon mass increases, and it is enhanced when the magnon mass decreases. We fit $z_{\text{com}}(t)$ in Fig. 3 to $\hbar|\partial_z f_{\text{Larmor}}|t^2/(2M^*)$ to estimate the effective mass M^* , where we assume that the effective magnetic moment μ^* is the same as that of a free atom μ and that the effective mass M^* is averaged over the density distribution and the momentum range. The estimated effective mass is $M^*/M \simeq 1.05$ and 0.97 for the red dashed curve and the green dot-dashed curve in Fig. 3, respectively, which are consistent with the dispersion relation in Fig. 2.

In conclusion, we have investigated the dynamics of magnons in a polarized spin-1 ^{87}Rb BEC using the mean-field theory with the MDDI. In the same situation as was used in the experiment [38], we have shown that the dispersion relation of a magnon lies below that of a free

atom, which agrees with the experiment. We have confirmed that the deviation mainly arises from the MDDI. We also proposed a simple modification to the experiment: when the direction of the magnetic field is changed from the long axis to the tight axis of the oblate condensate, the dispersion relation deviates to the upper side, and the effective mass of a magnon decreases. This effect can be observed with the current experimental precision. We have shown that the change in the magnon mass affects the acceleration dynamics of magnons in the field gradient. The acceleration is suppressed (enhanced) when the magnon mass is increased (decreased). Since our method can both increase and decrease the magnon mass, the difference in their acceleration dynamics may be detected even in the presence of the systematic error of the experiment.

Since the MDDI shift is already detectable for ^{87}Rb , magnons in BECs of ^{52}Cr , ^{164}Dy , and ^{168}Er are strongly affected by the MDDI. For example, for ^{52}Cr , the ratio between the MDDI and kinetic energies is $12^2 m_{\text{Rb}}/m_{\text{Cr}} \simeq 86$ times larger than the present case. The strong dipolar effect may exhibit a novel dynamics of magnons.

We thank G. Edward Marti for the experimental data and valuable comments. This work was supported by JSPS KAKENHI Grant Number 26400414 and by KAKENHI (No. 25103007, ‘‘Fluctuation & Structure’’) from MEXT, Japan.

-
- [1] J. Stuhler, A. Griesmaier, T. Koch, M. Fattori, T. Pfau, S. Giovanazzi, P. Pedri, and L. Santos, *Phys. Rev. Lett.* **95**, 150406 (2005).
- [2] S. E. Pollack, D. Dries, M. Junker, Y. P. Chen, T. A. Corcovilos, and R. G. Hulet, *Phys. Rev. Lett.* **102**, 090402 (2009).
- [3] G. Bismut, B. Laburthe-Tolra, E. Maréchal, P. Pedri, O. Gorceix, and L. Vernac, *Phys. Rev. Lett.* **109**, 155302 (2012).
- [4] M. Lu, N. Q. Burdick, S. H. Youn, and B. L. Lev, *Phys. Rev. Lett.* **107**, 190401 (2011).
- [5] T. Lahaye, T. Koch, B. Fröhlich, M. Fattori, J. Metz, A. Griesmaier, S. Giovanazzi, and T. Pfau, *Nature (London)* **448**, 672 (2007).
- [6] T. Koch, T. Lahaye, J. Metz, B. Fröhlich, A. Griesmaier, and T. Pfau, *Nat. Phys.* **4**, 218 (2008).
- [7] T. Lahaye, J. Metz, B. Fröhlich, T. Koch, M. Meister, A. Griesmaier, T. Pfau, H. Saito, Y. Kawaguchi, and M. Ueda, *Phys. Rev. Lett.* **101**, 080401 (2008).
- [8] J. Metz, T. Lahaye, B. Fröhlich, A. Griesmaier, T. Pfau, H. Saito, Y. Kawaguchi, and M. Ueda, *New J. Phys.* **11**, 055032 (2009).
- [9] K. Aikawa, A. Frisch, M. Mark, S. Baier, A. Rietzler, R. Grimm, and F. Ferlaino, *Phys. Rev. Lett.* **108**, 210401 (2012).
- [10] B. Pasquiou, E. Maréchal, G. Bismut, P. Pedri, L. Vernac, O. Gorceix, and B. Laburthe-Tolra, *Phys. Rev. Lett.* **106**, 255303 (2011).
- [11] Y. Eto, H. Saito, and T. Hirano, *Phys. Rev. Lett.* **112**, 185301 (2014).
- [12] K. Góral, L. Santos, and M. Lewenstein, *Phys. Rev. Lett.* **88**, 170406 (2002).
- [13] D. H. J. O’Dell, S. Giovanazzi, and G. Kurizki, *Phys. Rev. Lett.* **90**, 110402 (2003).
- [14] L. Santos, G. V. Shlyapnikov, and M. Lewenstein, *Phys. Rev. Lett.* **90**, 250403 (2003).
- [15] R. M. Wilson, S. Ronen, J. L. Bohn, and H. Pu, *Phys. Rev. Lett.* **100**, 245302 (2008).
- [16] R. W. Cherg and E. Demler, *Phys. Rev. Lett.* **103**, 185301 (2009).
- [17] N. R. Cooper, E. H. Rezayi, and S. H. Simon, *Phys. Rev. Lett.* **95**, 200402 (2005).
- [18] J. Zhang and H. Zhai, *Phys. Rev. Lett.* **95**, 200403 (2005).
- [19] R. M. W. van Bijnen, D. H. J. O’Dell, N. G. Parker, and A. M. Martin, *Phys. Rev. Lett.* **98**, 150401 (2007).
- [20] M. Klawunn, R. Nath, P. Pedri, and L. Santos, *Phys. Rev. Lett.* **100**, 240403 (2008).
- [21] W. E. Shirley, B. M. Anderson, C. W. Clark, and R. M. Wilson, *Phys. Rev. Lett.* **113**, 165301 (2014).
- [22] P. Pedri and L. Santos, *Phys. Rev. Lett.* **95**, 200404 (2005).
- [23] I. Tikhonenkov, B. A. Malomed, and A. Vardi, *Phys. Rev. Lett.* **100**, 090406 (2008).

- [24] R. Nath, P. Pedri, and L. Santos, Phys. Rev. Lett. **101**, 210402 (2008).
- [25] Y. Kawaguchi, H. Saito, and M. Ueda, Phys. Rev. Lett. **96**, 080405 (2006).
- [26] K. Gawryluk, M. Brewczyk, K. Bongs, and M. Gajda, Phys. Rev. Lett. **99**, 130401 (2007).
- [27] B. Sun and L. You, Phys. Rev. Lett. **99**, 150402 (2007).
- [28] S. Yi and H. Pu, Phys. Rev. Lett. **97**, 020401 (2006).
- [29] Y. Kawaguchi, H. Saito, and M. Ueda, Phys. Rev. Lett. **97**, 130404 (2006).
- [30] M. Takahashi, S. Ghosh, T. Mizushima, and K. Machida, Phys. Rev. Lett. **98**, 260403 (2007).
- [31] S. Hoshi and H. Saito, Phys. Rev. A **81**, 013627 (2010).
- [32] J. A. M. Huhtamäki and P. Kuopanportti, Phys. Rev. A **82**, 053616 (2010).
- [33] H. Saito, Y. Kawaguchi, and M. Ueda, Phys. Rev. Lett. **102**, 230403 (2009).
- [34] M. Yasunaga and M. Tsubota, Phys. Rev. Lett. **101**, 220401 (2008).
- [35] J. A. M. Huhtamäki and P. Kuopanportti, Phys. Rev. A **84**, 043638 (2011).
- [36] M. Vengalattore, S. R. Leslie, J. Guzman, and D. M. Stamper-Kurn, Phys. Rev. Lett. **100**, 170403 (2008).
- [37] Y. Kawaguchi, H. Saito, K. Kudo, and M. Ueda, Phys. Rev. A **82**, 043627 (2010).
- [38] G. E. Marti, A. MacRae, R. Olf, S. Lourette, F. Fang, and D. M. Stamper-Kurn, Phys. Rev. Lett. **113**, 155302 (2014).
- [39] T. -L. Ho, Phys. Rev. Lett. **81**, 742 (1998).
- [40] T. Ohmi and K. Machida, J. Phys. Soc. Jpn. **67**, 1822 (1998).
- [41] N. T. Phuc, Y. Kawaguchi, and M. Ueda, Ann. Phys. (Amsterdam) **328**, 158 (2013).
- [42] S. Giovanazzi, A. Görlitz, and T. Pfau, Phys. Rev. Lett. **89**, 130401 (2002).
- [43] Y. Kawaguchi, H. Saito, and M. Ueda, Phys. Rev. Lett. **98**, 110406 (2007).
- [44] W. H. Press, S. A. Teukolsky, W. T. Vetterling, B. P. Flannery, *Numerical Recipes*, 3rd ed, Sec. 20.7 (Cambridge Univ. Press, Cambridge, 2007).
- [45] See Supplemental Material at <http://link.aps.org/supplemental/...> for movies of the dynamics.
- [46] Since the initial one or two oscillations are used for fitting, ω obtained from the fitting is insensitive to the form of the fitting function.
- [47] From this consideration, the tight confinement in the y direction is not crucial for the frequency shift. In fact, for a trap with $(\omega_x, \omega_y, \omega_z)/2\pi = (50, 50, 4)$ Hz, we obtain the frequency shift similar to Fig. 2.